J Appl Electrochem (2013) 43:453–465
DOI 10.1007/s10800-013-0530-9

ORIGINAL PAPER

CFD evaluation of internal manifold effects on mass transport distribution in a laboratory filter-press flow cell

L. Vázquez · A. Alvarez-Gallegos · F. Z. Sierra · C. Ponce de León · F. C. Walsh

Received: 5 August 2012 / Accepted: 24 January 2013 / Published online: 7 February 2013

Abstract The internal manifold geometry strongly influences the flow distribution inside an electrochemical reactor. The mass transport coefficient is a function of the flow pattern and is a key parameter in successful electrochemical reactor design and scale-up. In this work, a commercial computational flow dynamics (CFD) package was used to describe the flow pattern in the FM01-LC reactor at controlled volumetric flow rates (corresponding to mean linear flow velocities past the electrode surface between 0.024 and 0.11 m s^{-1}). Numerical *Re* numbers were obtained for each local flow velocity at different positions in the reactor channel. From a known mass transport correlation (based on dimensionless groups, i.e. *Sh*, *Re*, *Sc*), numerical k_m values were obtained (in the range $200 < Re < 1{,}000$) at different positions in the reactor channel. Computed k_m numbers are compared against experimental values. This computational approach could be useful in reactor design or selection since it facilitates a fast, preliminary reactor flow and mass transport characterisation without experimental electrochemical measurements.

L. Vázquez · A. Alvarez-Gallegos · F. Z. Sierra
Research Center in Engineering and Applied Sciences, Autonomous University of Morelos, Av. Universidad 1001, 62051 Cuernavaca, Morelos, Mexico

A. Alvarez-Gallegos (✉)
Universidad Autónoma del Estado de Morelos, Av. Universidad 1001 Col. Chamilpa, 62209 Cuernavaca, Morelos, Mexico
e-mail: aalvarez@uaem.mx

C. P. de León · F. C. Walsh
Electrochemical Engineering Laboratory, Energy Technology Research Group, Engineering Sciences, University of Southampton, Highfield, Southampton SO17 1BJ, UK

Keywords CFD · Channel flow · Filter-press cell · Mass transport · Parallel plates

List of symbols

A	Active electrode area, m^2
A_{hole}	Cross-sectional area of an individual hole in Eq. (12), m^2
B	Channel width, m
D	Diffusion coefficient of cupric ions, m^2 s^{-1}
D_e	Cell equivalent diameter in Eq. (8), m
a, b, c, e	Empirical constant in Eqs. (1), (2), (18)–(22), dimensionless
c	Concentration of electroactive species i in the bulk electrolyte, mol m^{-3}
d_e	Equivalent hydraulic diameter of the rectangular flow channel, dimensionless
F	Faraday constant, 96,485 C mol^{-1}
I_L	Local limiting current, A
i, j	Counters in Eqs. (13)–(17), dimensionless
k_m	Local mass transport coefficient, m s^{-1}
$k_{numerical}$	Mass transport coefficient values predicted by CFD model, Eq. (25), m s^{-1}
k_{exp}	Experimental values of mass transport coefficient, Eq. (25), m s^{-1}
L	Electrode length, m
N_i	Flux of electroactive species i, mol m^{-2} $s^{-1)}$
n_h	Number of holes per row in Eq. (11), dimensionless
n_r	Number of rows in the flow distribution manifold in Eq. (11), dimensionless
p	Pressure in Eq. (14), Pa
R	Molar gas constant, J K^{-1} mol^{-1}
s	Cross-sectional area of the flow inlet in Eq. (9), m^2
S	Cross-sectional area of the cell in Eq. (9), m^2
T	Temperature, K

v Local mean linear flow velocity predicted by CFD, m s^{-1}
$\bar{v}$ The characteristic linear flow velocity, the ratio of mean volumetric flow rate to the cross-sectional area of the electrolyte channel, m s^{-1}
x, y, z Natural coordinate axes, –
z_i Charge of species i, dimensionless
γ Aspect ratio in Eq. (10), dimensionless
δ_N Nernst diffusion layer thickness, m
ρ Electrolyte density, kg m^{-3}
μ Dynamic electrolyte viscosity, kg m^{-1} s^{-1}
τ Viscous stress term, N

Dimensionless groups

Re Reynolds number, dimensionless
Sc Schmidt number, dimensionless
Sh Sherwood number, dimensionless
λ Constant describing the geometrical arrangement of holes in the flow distributor in Eq. (11), dimensionless
ξ Ratio of whole area of the electrode channel to the manifold cross-sectional area in Eq. (12), dimensionless

1 Introduction

The successful scale-up of parallel plate electrochemical reactors often includes the analysis of dimensionless groups which describe their geometric, kinematic, thermal, chemical and electrical characteristics [1]. Accordingly, mass transport and fluid dynamics are amongst the main considerations during a reliable scale-up procedure [2–5].

The hydrodynamic behaviour of a parallel plate reactor usually involves flow through a rectangular channel and the flow pattern is strongly linked to the mass transport coefficient (k_m) according to a power law expression [3]

$$k_m = a(\bar{v})^b \tag{1}$$

where $\bar{v}$ is the characteristic linear flow velocity, the ratio of the mean volumetric flow rate to the cross-sectional area of the electrolyte channel; a and b are empirical constants. k_m and the empirical constants can be evaluated in a rectangular channel from dimensionless group correlations [3, 6, 7]. The mass transport coefficient is a function of fluid flow conditions and the transport properties of the electrolyte. Mass transport correlations may be written in the following general form [1, 3]:

$$Sh = aRe^b Sc^c\ Le^e \tag{2}$$

where *Sh* is the Sherwood number, *Re* is the Reynolds number, *Sc* is the Schmidt number and the dimensionless length group, *Le* is the ratio of hydraulic diameter to the length of the electrode in the direction of the flow, and a, b and c are empirical constants.

In academic studies, electrochemical flow cells are normally designed to have a calming zone between the electrolyte entrance and the electrodes to ensure a fully developed flow [1, 3]. Under these conditions, fluid flow behaviour is completely described by the Navier–Stokes and momentum conservation equations [1]. For these simple cases, and taking into account appropriate assumptions, a set of such equations can be analytically solved and several correlations are available as a function of the depth/width aspect ratio S/B of the flow channel [1, 3, 8].

During the design of pilot- and industrial-scale electrochemical reactors, fully developed flow is rare because manifolds usually inject or extract the electrolyte very close to the electrodes to realise compact designs or to induce turbulent flow [9]. For these cases, a successful mass transport evaluation is carried out experimentally using Eq. (1). The volumetric flow rate is experimentally measured with a flow metre, and a log-log plot of k_m versus $\bar{v}$ should be linear and of slope b. Although this procedure can provide a highly accurate approximation of the reactor performance, it is expensive (several reactors need to be constructed and evaluated before an appropriate one is selected), time consuming and depends greatly on available experimental skills and facilities.

The objective of this work is to explore the feasibility of using computational fluid dynamics (CFD) as a tool to evaluate the manifold effects on mass transfer in developing flow along an electrochemical reactor. In this way, for a particular electrochemical reactor, the main transport properties of an electrolyte as a function of the manifold design are obtained by numerical simulation without any experimentation. This method will be compared against other available tools. The well-known ICI FM01-LC electrochemical reactor was chosen as a model reactor since it was designed to provide laboratory data, facilitating scale-up [2]. A number of papers on the characterisation of the reaction environment in this cell have been published previously [2, 10–18]. The FM01-LC reactor has been fully described in the references provided and reviewed by Walsh and Robinson [19]; the most important geometrical characteristics of the flow channel are summarised in Fig. 1 including (a) the inlet manifolds and (b) the main geometrical details (projected electrode area 0.0064 m^2).

2 Theoretical considerations

2.1 Assessment of flow regime

Mechanical similarities between two flows exist if their Reynolds numbers are equal for both flows [1]. Therefore,

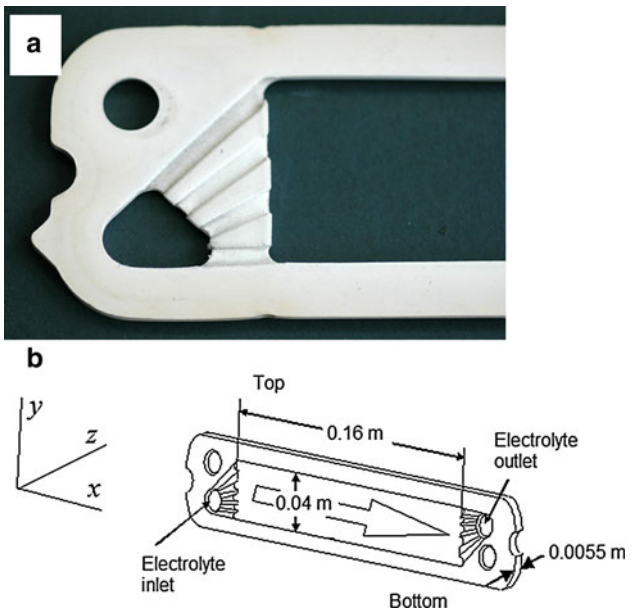

Fig. 1 Part of the length of the flow channel in the FM01-LC electrolyser, showing **a** the inlet manifold and **b** the electrolyte ports leading to the *rectangular* cross section flow channel

fluid flow similarity is a key consideration for a reliable scale-up electrochemical reactor procedure. In this way, the Reynolds number defines the flow conditions in a particular electrochemical reactor geometry. All flows encountered in engineering practice become unstable above a certain Reynolds number, known as the critical Reynolds (Re_{crit}). At low Reynolds numbers ($Re < Re_{crit}$), flows are laminar and at higher Reynolds numbers ($Re > Re_{crit}$), flows are turbulent. In the laminar regime, the flow is smooth and adjacent layers of fluid slide past each other in an orderly fashion. Moreover, if the applied boundary conditions do not change with time, the flow is steady. On the other hand, turbulent flow behaviour is radically different and motion becomes intrinsically unsteady even with constant boundary conditions imposed. Direct visualization of turbulent flow reveals rotational flow structures (turbulent eddies) having a wide range of length scales. In general, in both industrial and laboratory electrochemical reactors, the laminar regime is preferred to the turbulent regime because, in the first case, the hydrodynamic behaviour is easier to understand. Additionally, the laminar regime requires less energy for pumping the fluid through an electrochemical reactor.

The numerical value of Re_{crit} is not a constant and it depends quite strongly on the geometry of manifolds to introduce the fluid and to remove it from a duct (pipe, channel, etc.). Therefore, the precise Re_{crit} value at which the flow conditions become turbulent is very important. The following criteria have been employed either to assess the minimum downstream length required for a fully developed flow or to find a suitable model to explain fluid flow behaviour which would lead to a reliable scale-up procedure for filter-press electrochemical reactors.

2.2 Entrance length

According to the literature [20, 21], the minimum downstream length required for a fully developed flow can be evaluated using the following expressions

$$\text{Laminar flow } L^* = 0.06\, Re\, d \quad (3)$$

$$\text{Turbulent flow } L^* = 4.4\, Re^{0.167}\, d \quad (4)$$

$$\text{Turbulent flow } L^* = (20\ to\ 40)\, d \quad (5)$$

$$\text{Turbulent flow (Channel) } L^* = (20 \text{ to } 100)\, d_e \quad (6)$$

$$\text{Turbulent flow (Channel) } L^* = 6\, d_e \quad (7)$$

where L^* is the minimum entrance length, d is the diameter of a circular pipe and d_e is the hydraulic diameter of a channel. As it can be seen from the above equations, the evaluation of L^* is only a function of two parameters: the dimensionless Re number and the diameter (or hydraulic diameter). The first one is evaluated by taking into account the characteristic linear flow velocity ($\bar{v}$) and the second one is related to the channel cross-sectional area. Under these conditions, the flow behaviour differences between electrode surface and bulk solution as well as near manifolds are ignored. Therefore, the main drawbacks of those criteria are their inconsistencies as was recognized [20].

2.3 Flow dispersion models

In principle, most filter-press reactors can be considered plug flow reactors due their geometrical characteristics. Under ideal conditions, the hydrodynamic behaviour of these reactors can be described by a Dirac delta function: an instantaneous impulse at the cell inlet should pass along the reactor and be detected at the cell outlet without alteration [22]. This implies that the residence time for all chemical species is the same and there is no mixing in the direction of flow. Such ideal behaviour is never reached and deviations are observed due to manifold geometry and velocity fluctuations. The approach may be used to evaluate the flow pattern within the FM01-LC [14, 16]. It has been recognized that there are inherent difficulties in the application of this flow model, and the appearance of tailing in the tracer curves leads to error [23, 24]. In order to minimize the tailing phenomenon, colourants may be employed to assess the flow pattern [25, 26]. However, the main drawbacks of these approaches are (1) the necessity to have an electrochemical reactor to evaluate then assess its flow pattern and (2) this information is not sufficient to

better understand how the flow pattern affects the spatial distribution of mass transfer rates.

2.4 Dimensionless groups describing flow, mass transport and electrolyte transport

The sudden expansion of fluid flow is a more convenient method to introduce the electrolyte to an electrochemical reactor. As a result, at the cell entrance, the flow pattern is characterised by the presence of recirculating fluid. Hence, the Reynolds number is a function of the expansion geometry and several attempts were made to evaluate this phenomenon. In general, the method consists of correlating the flow expansion factor (due to changes in the manifold geometry) with a measurable quantity such as heat [27–30] or mass transfer coefficients [31–34]. From some of these works [29, 32], the following general mass transport correlation was obtained as a function of different entry arrangements:

$$Sh\ Sc^{-1/3} = 0.11 Re^{0.73} (d_e/D_e)^{-1} \tag{8}$$

where d_e/D_e is the ratio of entrance to the electrochemical cell, the equivalent diameter. In general, Eq. (8) agrees well with experimental data, as long as the cell entry is limited to one circular bore whole. Unfortunately, Eq. (8) cannot be used for different manifold designs, e.g. a slit-type cell entrance. For this reason, Eq. (8) was improved by introducing a new expansion factor s/S [35], where s and S are the cross-sectional areas of the entrance and the cell, respectively. The following empirical correlation was found to be valid for both tube-type entrance and slit-type entrance and $400 < Re < 3{,}500$

$$Sh\ Sc^{-1/3} = 0.068 Re^{0.72} (s/S)^{-1/2} \tag{9}$$

Although Eq. (9) appeared to work well for the manifolds previously described, it fails when applied to the FM01-LC electrolyser (Fig. 1) because it does not take into account the distribution, number and type of ports.

In an attempt to solve the problem, a geometrical manifold parameter ψ was proposed recently [7]. The dimensionless group ψ is more developed than those described previously since it includes geometrical details of the manifold design such as thickness, width, distribution of the open spaces and the free area for the electrolyte entrance within the electrochemical reactor. Mathematically, the manifold parameter is expressed as

$$\psi = \frac{\gamma\, d_e}{L\, \lambda\, \xi} \tag{10}$$

where γ is the aspect ratio, d_e is the equivalent diameter, L is the channel length, λ considers the geometrical arrangement of the holes in the flow distributor and ξ is the free area for liquid entrance within the reactor (expressed as the ratio of whole area of the electrode channel to the manifold cross-sectional area). These geometrical parameters can be mathematically defined by the following equations:

$$\lambda = \frac{n_h n_r}{\gamma} \tag{11}$$

$$\xi = \frac{n_h n_r A_{hole}}{BS} \tag{12}$$

where n_h is the number of identical holes in one row, n_r is the number of rows in the distribution manifold and A_{hole} is the cross-sectional area of an individual hole. According to the authors, Eqs. (10)–(12) can be interpreted as follows: large values of ψ are associated with pronounced entrance/exit effects and high mass transport rate; in a similar way, high values of Sh are associated with low values of ξ. For a well-designed reactor, the ideal performance (low entrance/exit effects) value of ξ is 1. However, for $\xi < 1$, a jet stream is expected at the cell inlet. Applying this method to the FM01-LC, the following numerical results are found: $\psi = 0.0027$, $\xi = 0.105$. Using this information, the following diagnosis for the FM01-LC can be made: (i) the electrochemical cell design is far from ideal ($\xi = 0.105$) and (ii) at the cell entrance, jet stream, vortex and a high mass transport rate are expected. Although this information may be useful for an experienced designer, for others, it is very subjective. In fact, for a theoretical design of an electrochemical reactor, the following key questions remain open: What is the minimum required length of the calming zone to subdue disturbances? How does the flow pattern affect the rate of mass transfer inside and out of the calming zone? In general, these questions can be answered by constructing then experimentally evaluating the rate of mass transfer at several points inside the electrochemical reactor. During this task, the parameters (ψ and ξ) are often, and incorrectly, considered as a minor detail or ignored by the designer.

3 Computational fluid dynamics

For over 20 years, CFD has been regarded as a feasible tool for reactor designing purposes. CFD has been employed to investigate flow patterns in empty [36] and spacer-filled rectangular channels [37]. At present, CFD offers the possibility for evaluating, under realistic conditions, the flow pattern and its effect on mass transport in developing fluids along a reactor [17, 18, 38–40]. In the present study, Fluent (v6) was used to provide a numerical description of the flow patterns in the FM01-LC reactor working under similar experimental conditions to those documented elsewhere [10].

3.1 Modelling the flow pattern along the FM01-LC electrolyser

The electrolyte is distributed to the reactor channel by internal manifolds incorporated within the cell spacers as shown in Fig. 1. When the electrolyte is pumped through the channel from left to right, a flow pattern develops along the channel length as a function of the flow rate. The fluid flow can be modelled from the basic principles of conservation of mass, momentum and energy [41] and the most important conditions are summarised in the following sections.

3.2 Modelling conditions

The main modelling conditions are fed via a pre-processor (Gambit®). It is estimated that perhaps 50 % of the time spent in a CFD project is devoted to suitable definition of the domain geometry and grid generation. At this stage, the following activities are normally carried out:

- Definition of the FM01-LC reactor geometry (the computational channel volume is taken as 35.2 cm^3).
- Subdivision of the geometry into non-overlapping 206,272 tetrahedral cells via grid generation.
- Definition of fluid properties (see Table 1) and selection of appropriated boundary conditions such as the electrolyte mass flux (kg s^{-1}) at the main entrance of the reactor channel (before the inlet manifold), see Table 2.

3.3 Governing equations of fluid flow

In three dimensions, fluid flow can be described by a system of five partial differential equations: mass conservation, x, y and z momentum equations and the energy balance equation. In this work, the following considerations are taken into account: (i) steady state is assumed in the fluid flow equations, whilst the time variable is not considered; (ii) the temperature, density and viscosity of the fluid are constant; (iii) natural convection is neglected due to the predominance of forced convection; and (iv) there is no linkage between the energy equation, the mass conservation and the momentum equations. As a consequence, the system is reduced to four partial differential equations, describing fluid flow in three dimensions. The energy equation needs to be solved alongside the others if the problem involves heat transfer. In a laminar regime, fluid flow behaviour is completely described by the Navier–Stokes equations:

$$\frac{\partial v_i}{\partial x_i} = 0 \tag{13}$$

$$\frac{\partial}{\partial x_i}(v_i v_j) = -\frac{\partial}{\partial x_j} p\delta_{ij} + \frac{\partial}{\partial x_j}\tau_{ij} \tag{14}$$

where v_i, x_i are the velocity vector and its position ($i = x, y, z$), respectively, p is the pressure and τ is a viscous stress term.

As noted previously, the set of such equations can be analytically solved for simple cases [1, 41]. However, all flows encountered in engineering practice become unstable above the critical Reynolds number. Therefore, flows of engineering significance are often turbulent and fluid engineers need access to viable tools capable of describing the effects of turbulence at Reynolds numbers well below 2000. In order to overcome the problem, commercial CFD packages offer the possibility of using turbulence models that can be solved in three dimensions alongside the Navier–Stokes equations.

It is expected that as the fluid flows through the channel entrance, some vortexing and four jets are formed as a result of the flow distributors. Consequently, the renormalization-group (RNG) model was chosen for modelling the fluid flow through the channel, shown in Fig. 1. The RNG model was used to solve terms that appear when the set of Navier–Stokes equations is applied to flow regions which are dominated by strong velocity gradients, like vortex flows that characterise recirculation flow regions or boundary layer separation flows. The RNG model has been used before for similar hydrodynamic situations [38]. A detailed description of the RNG model and how it interacts with the Navier–Stokes Eqs. (13) and (14) can be found elsewhere [41, 42].

Table 1 Physical and transport properties of the electrolyte

Property	Value
Fluid density, ρ	1,096 kg m^{-3}
Dynamic viscosity, μ	0.00119 kg m^{-1} s^{-1}
Schmidt number, $Sc = \mu/\rho\, D_{Cu^{2+}}$	2,172
Diffusion coefficient of Cu^{2+}, $D_{Cu^{2+}}$	5.0×10^{-10} m^2 s^{-1}
Reynolds number, $Re = v_\infty \rho\, d_e/\mu$	197–918

4 Experimental details

4.1 Simulation of fluid flow

Once the complete geometrical description of the FM01-LC reactor was fed to the CFD package via the interface

Table 2 Characteristic linear flow velocities of the electrolyte and the Reynolds number for the FM01-LC electrolyser

Characteristic linear flow velocity in the channel, v/m s^{-1}	0.024	0.032	0.048	0.065	0.081	0.096	0.112	0.192
Nominal Reynolds number, Re	197	262	393	533	664	787	918	1,574

pre-processor, the numerical solution is carried out using the solver interface based on a finite volume approach. The following steps are performed: (i) integration of governing equations of fluid flow over all the (finite) control volumes of the domain, (ii) conversion of the resulting integral equations into a system of algebraic equations and (iii) solution of algebraic equations by an iterative procedure.

The boundary conditions were defined as inlet conditions according to the physical properties of the electrolyte given in Table 1 [10] and the experimental mass flow rate (measured with the flow-metre via mean volumetric flow rate), rather than characteristic linear flow velocities, given in Table 2 [10]. *Re* numbers in Tables 1 and 2 were evaluated taking into account the characteristic linear flow velocity. A detailed numerical description of the flow pattern as a function of the characteristic linear flow velocity along the FM01-LC length is given elsewhere [17, 18]. Figure 2a shows a general overview of how the electrolyte develops over the first four centimetres into the channel reactor at the lowest characteristic linear flow velocity (0.024 m s^{-1}). In contrast, Fig. 2b shows a similar situation for the highest characteristic linear flow velocity (0.192 m s^{-1}). As can be seen from Table 2 and Fig. 2, Reynolds numbers are nominally all in the laminar regime studied here. However, some strong velocity gradients (due to vortexing and jet flows) are evident over the whole range of characteristic linear flow velocities considered in this study. Modelling unstable flows at turbulent regimes is known to be especially challenging [43, 44]. Therefore, the RNG turbulent model was solved alongside the Navier–Stokes equations over the entire range of characteristic linear flow velocities.

4.2 Mass transport and fluid dynamics

As discussed in the introduction, an idealised reactor design requires fully developed flow conditions before the electrolyte contacts the electrode surface. The main parameters such as the Nernst diffusion layer thickness (δ_N), the local mass transport coefficient (k_m) and the limiting current (I_L) should be uniform before contacting the electrode surface. As there is currently no mathematical equation that links the mass transport coefficient and the hydrodynamic behaviour for developing flows in a channel, the use of alternative routes is justified. The following section discusses how the flow pattern is substituted into a set of general mass transport correlations to calculate the mass transport coefficients.

4.3 Modelling mass transport

The hydrodynamic behaviour within the FM01-LC reactor influences the mass transport coefficient and the electrode current when the process is mass transport controlled. In this study, it was always assumed that a Nernst stagnant diffusion layer of thickness δ_N developed near the electrode surface as shown in Fig. 3.

Where c is the concentration of the electroactive species i, A is the electrode area, I_L is the transport-controlled current, n is the number of electrons in the electrode reaction as written, F is Faraday constant, k_m is local mass transport coefficient and N is the flux of electroactive species, which is defined as [45]

$$N_i = -D_i \nabla c_i - \frac{z_i F}{RT} D_i c_i \nabla \phi + c_i \mathbf{v} \tag{15}$$

Therefore, the flux of electroactive species i depends on their diffusion (first term on the right-hand side), migration (second term on the right-hand side) and convection (last term). In order to solve Eq. (15), the following assumptions are taken into account:

(1) Steady state is assumed during electrolyser operation.
(2) The migration term can be neglected because the solution contains an excess of supporting electrolyte.
(3) In the bulk solution, the diffusion term can be neglected and a realistic flow pattern can be obtained by applying a CFD technique (the solution of the Navier–Stokes equations coupled with the RNG model). This implies a uniform concentration in the bulk solution.
(4) In the Nernst stagnant diffusion layer, convection can be neglected and its thickness is determined by the flow velocity in the outer edge of the boundary layer. In the diffusion layer, N_i can be expressed in terms of one-dimensional linear molecular diffusion [1]. Therefore, the flux of electroactive species to the electrode surface is expressed by

$$N_i = \frac{D_i}{\delta_N}(c_0 - c) \tag{16}$$

where c_0 and c are the bulk concentration and concentration, respectively, at the electrode surface of the species i; the mass transfer coefficient, k_m, can be expressed as [1]

$$k_m = \frac{D_i}{\delta_N} \tag{17}$$

Conversely, mass transport in electrochemical systems is often cast in terms of dimensionless numbers. Thus, dimensionless flux (*Sh*) is a function of the dimensionless fluid velocity (*Re*) multiplied by the dimensionless fluid properties (*Sc*). In forced convection reactors, this correlation is often written in the form of Eq. (2).

Consequently, if the first supposition is true, mass transfer coefficient in the FM01-LC must simultaneously satisfy both Eqs. (2) and (16).

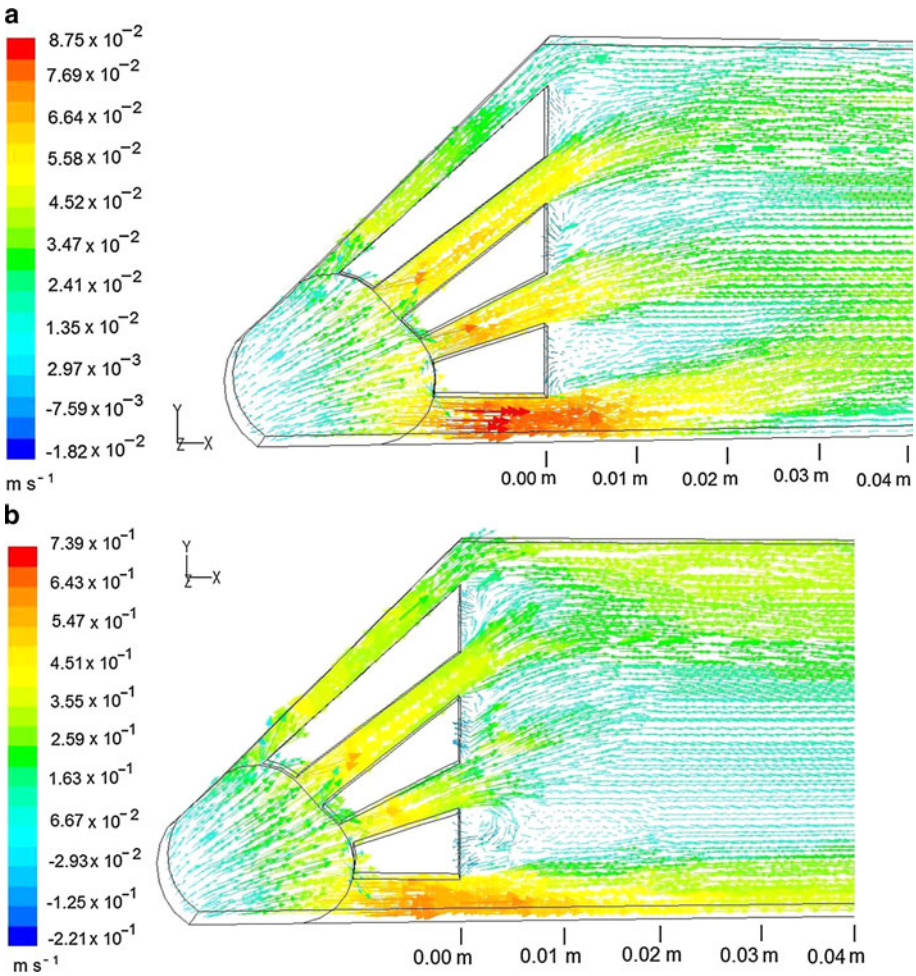

Fig. 2 A numerical description of the fluid flow development along the first 4 cm of the channel length. **a** Mean linear flow velocity = 0.0.024 m s^{-1}. **b** Mean linear flow velocity = 0.0.192 m s^{-1}

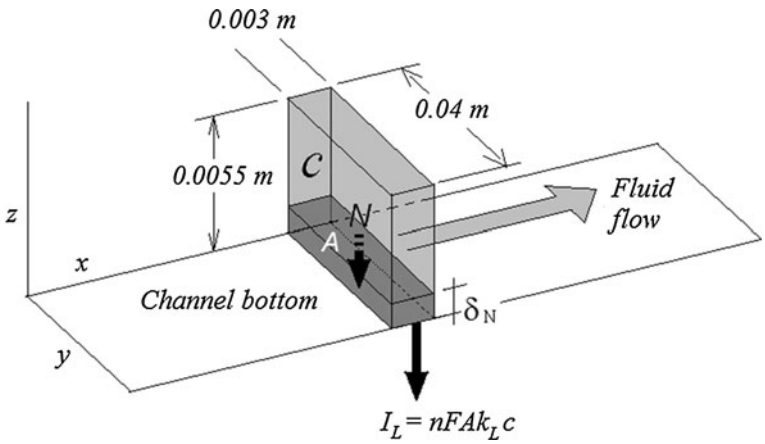

Fig. 3 The idealised flow along the channel, showing development of the Nernst diffusion layer thickness, δ_N. N is the flux of reactant towards the electrode surface, perpendicular to the flow direction. I_L is the convective-diffusion limiting current for a concentration c, whilst k_m is the mass transport coefficient over electrode area A

If a realistic flow pattern is obtained from numerical calculation and an appropriated mass transport correlation is chosen for a given electrochemical reactor, then the mass transport coefficient (k_m) can be numerically evaluated via the *Sh* number definition, as given by Eq. (2). For parallel plate reactors (including the FM01-LC one) working at $60 < Re < 2{,}000$, selected dimensionless group correlations (Eqs. 18 to 22) are provided in Table 3.

Equations (18)–(22) were coupled with the theoretical flow pattern obtained at different volumetric flow rates. It was then possible to estimate the dimensionless groups *Re*, *Sh* and k_m at different positions in the FM01-LC reactor

Table 3 Selected mass transport correlations for fluid flow through parallel plate reactors at $60 < Re < 2{,}000$

Equation	$Sh = a\mathrm{Re}^b Sc^c Le^e$				Conditions	References
	a	b	c	e		
(18)	2.54	0.33	0.33	0.33	Fully developed laminar flow. $58 < Re < 2{,}000$, $2{,}850 < Sc < 5{,}140$, $0.17 < Le < 12.5$, $S/B = 0.167$ or 0.175	[3, 18]
(19)	1.85	0.33	0.33	0.33	Theoretical derivation for fully developed laminar flow assuming infinitely wide electrodes $ReSc\ (d_e/L) > 10^4$ and $Le \leq 35$	[3]
(20)	0.38	0.68	0.33		Baffled parallel plate reactor. Electrode area: 225 cm^2, $Le = 15$ cm/2.3 cm = 6.5	[46]
(21)	0.39	0.58	0.33		Flat plate, $70 < Re < 800$ $Sc = 1{,}572$, $L_e/d_e = 13$	[3]
(22)	0.22	0.71	0.33		FM01-LC reactor, $200 < Re < 1{,}000$ $Le = 16$ cm/0.967 cm = 16.6 Electrode area: 64 cm^2	[10]

The numbering of these correlations follows sequentially from Eqs. (1)–(17)

channel by taking into account the above assumptions, together with the following one: Although the fluid flow is not fully developed, it is considered to be sufficiently uniform to apply to Eqs. (18)–(22) at all volumetric flow rates considered in Table 2.

Local mass transport coefficients were evaluated considering an array of 100 × 32 imaginary segmented electrodes across the channel width and length. Figure 4 shows some of them at 0.01, 0.04 and 0.08 m from the channel entrance. Accordingly, a surface of 0.003 m length × 0.00035 m width was considered for each imaginary segmented electrode and the separation between them was 0.00005 m along the channel width.

An imaginary channel volume (0.003 m × 0.00035 m × 0.0055 m = 5.8 × 10^{-9} m^3) is linked to the surface of each segmented electrode. For each volume, a theoretical velocity profile was obtained with 10 local flow velocities along the channel depth (z dimension). For each velocity profile, an arithmetical average fluid velocity was obtained and it was considered to be the local mean flow velocity (v) representative of its volume.

A local mean Re was computed, for each corresponding local mean flow velocity (v), according to

$$Re = \frac{v\, d_e}{\nu} \tag{23}$$

For a given mass transport correlation (see Table 3), a local mean Sh was computed, from Eqs. (18) to (22), for each corresponding local mean flow velocity (v) and local mean Re.

For each corresponding local mean Sh obtained, an average k_m value was computed from Eq. (24) and was considered as the averaged k_m to be observed on the corresponding electrode surfaces.

$$k_m = D\left(\frac{Sh}{d_e}\right) \tag{24}$$

The differences between numerical and experimental mean mass transport coefficients were calculated according to

$$\mathrm{RE} = \left(1 - \frac{k_{\mathrm{numerical}}}{k_{\mathrm{exp}}}\right) \times 100 \tag{25}$$

where RE is the percentage relative error [47].

5 Results and discussion

5.1 General

From the detailed description of the numerical flow pattern in the FM01-LC reactor discussed elsewhere [17], it can be seen that fluid flow cannot develop for several major reasons: (a) Manifolds are not located at the centre of the channel depth and (b) the manifold geometry consist of four non-symmetrical rectangular ducts angled across the cell entrance and they are inverted at the channel entrance and exit. Consequently, the formation of vortexes and jets is observed and the fluid streams gradually shift from the bottom to the top of the channel, creating a low velocity region at the centre of the cell. Accordingly, mass transport coefficient will vary following the hydrodynamic behaviour observed across the whole range of nominal Re considered in Table 2. At low Re values, however, a more uniform k_m distribution along the channel width and length is expected as the fluid is moving away from the channel entrance. In this section, a summary of the numerical evaluation of k_m, estimated from the best equations shown

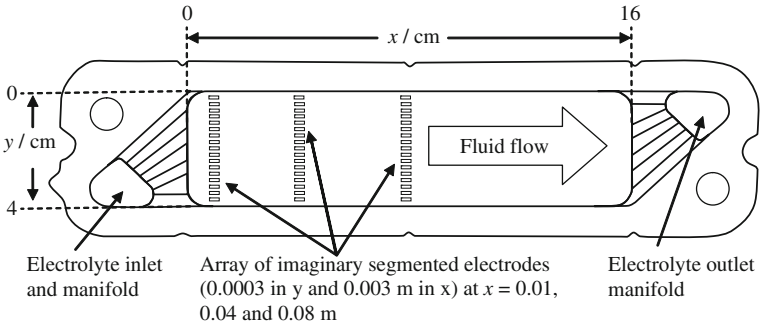

Fig. 4 The flow channel, showing the positions of imaginary segmented electrodes (surface of 0.003 m length × 0.0003 m width) at $x = 0.01$, 0.04 and 0.08 m from the channel entrance together with the *inlet* and *outlet* ports

in Table 3, corresponding to three columns of 100 imaginary electrodes each and located at 0.01, 0.04 and 0.08 m from the channel entrance, will be analysed and discussed at different flow velocities.

5.2 Mean linear flow velocity, $v = 0.024$ m s^{-1}

The effect of the manifold configuration on the mass transport coefficient is presented in Fig. 5a. From this graph, a set of local mean mass transport coefficients, corresponding to a column of 100 imaginary electrodes along the channel width, at 1 cm from the channel entrance can be seen. It can be seen that k_m predictions from Eqs. (18) and (21) agree reasonable well when compared with k_m obtained from Eq. (22). Noticeable differences can be seen at the jet and vortex positions, but RE does not exceed 19 % in the worst cases, for both mass transport correlations.

If an imaginary electrode, 0.003 m length and 0.04 m width, is considered, the following arithmetical average of k_m is obtained: Eq. (21), averaged $k_m = 6.27 \times 10^{-4}$ cm s^{-1} and Eq. (18), averaged $k_m = 7.67 \times 10^{-4}$ cm s^{-1}. When these values are compared against the experimental one, 7.66×10^{-4} cm s^{-1} [10], the following RE values of 18 and −0.13 % are obtained using Eqs. (21) and (18), respectively.

Using the same procedure, Fig. 5b shows a set of local mean mass transport coefficients along the channel width at 4 cm from the channel entrance. As expected, a more uniform k_m distribution along the channel width was obtained. In general, Eq. (21) tended to underestimate the k_m values (RE ≈ 10 %), whilst Eq. (18) overestimates them (RE ≈ 13.7 %). For an imaginary electrode, 0.003 m length and 0.04 m width, Eq. (21) gives an averaged $k_m = 6.11 \times 10^{-4}$ cm s^{-1} (RE of 20 % against the experimental value of 7.66×10^{-4} cm s^{-1}), whilst Eq. (18) gives an averaged $k_m = 7.72 \times 10^{-4}$ cm s^{-1} (RE of −0.75 % against the experimental value).

Figure 5c shows the corresponding set of k_m values at 8 cm from the channel entrance. At this distance, fluid flow is considered developed and the set of k_m is uniform, except near the channel boundaries where the wall effects are noticeable. In general, both Eqs. (21) and 18) give similar RE values of 11 and −9.4 %, respectively. For an imaginary electrode (0.003 m length and 0.04 m width), the following k_m values are obtained: Eq. (21), averaged $k_m = 6.43 \times 10^{-4}$ cm s^{-1} (RE of 16 % against the experimental 7.66×10^{-4} cm s^{-1}) and Eq. (18), averaged $k_m = 7.99 \times 10^{-4}$ cm s^{-1} (RE of 4.3 % against the experimental value). The conclusion so far is that at low nominal *Re*, the effect of the manifold configuration on the mass transport coefficient is best estimated by Eq. (18), see Table 3.

5.3 Mean linear flow velocity, $v = 0.065$ m s^{-1}

Under these hydrodynamic conditions, turbulent structures (jets and vortex) are increased and for the first third of the channel length, a non-uniform k_m distribution is expected. Figure 6a shows the corresponding set of $k_m = 1$ cm from the channel entrance. Noticeable differences in the calculations are found at jet positions where the maximum REs are 28.5 and 47 %, corresponding to Eqs. (21) and (18). For an imaginary electrode (0.003 m length and 0.04 m width), the following values are obtained: Eq. (21), averaged $k_m = 1.20 \times 10^{-3}$ cm s^{-1} (RE of 22 % against the experimental 1.54×10^{-3} cm s^{-1}) and Eq. (18), averaged $k_m = 1.09 \times 10^{-3}$ cm s^{-1} (RE of 29 % against the experimental value).

Figure 6b shows a set of local mean mass transport coefficients along the channel width at 4 cm from the channel entrance. Except for the location strongly affected by the biggest jet, near the bottom wall (4 cm. in x direction, 3.55 cm. In the y direction), the rest of the k_m values are almost uniform and both Eqs. (18) and (21) give similar values of RE ≈ 19 %, with respect to Eq. (22). For an imaginary electrode (0.003 m length and 0.04 m width), the following values are obtained: Eq. (21), averaged $k_m = 1.12 \times 10^{-3}$ cm s^{-1} (RE of 27.3 % against the experimental value 1.54×10^{-3} cm s^{-1}) and Eq. (18), averaged $k_m = 1.05 \times 10^{-3}$ cm s^{-1} (RE of 31.8 % against the experimental value).

Figure 6c shows the corresponding set of k_m values at 8 cm from the channel entrance. At this distance, fluid flow is considered developed and the set of k_m is uniform, except near the channel boundaries where the wall effects are present. Both Eq. (21) and Eq. (18) give similar RE

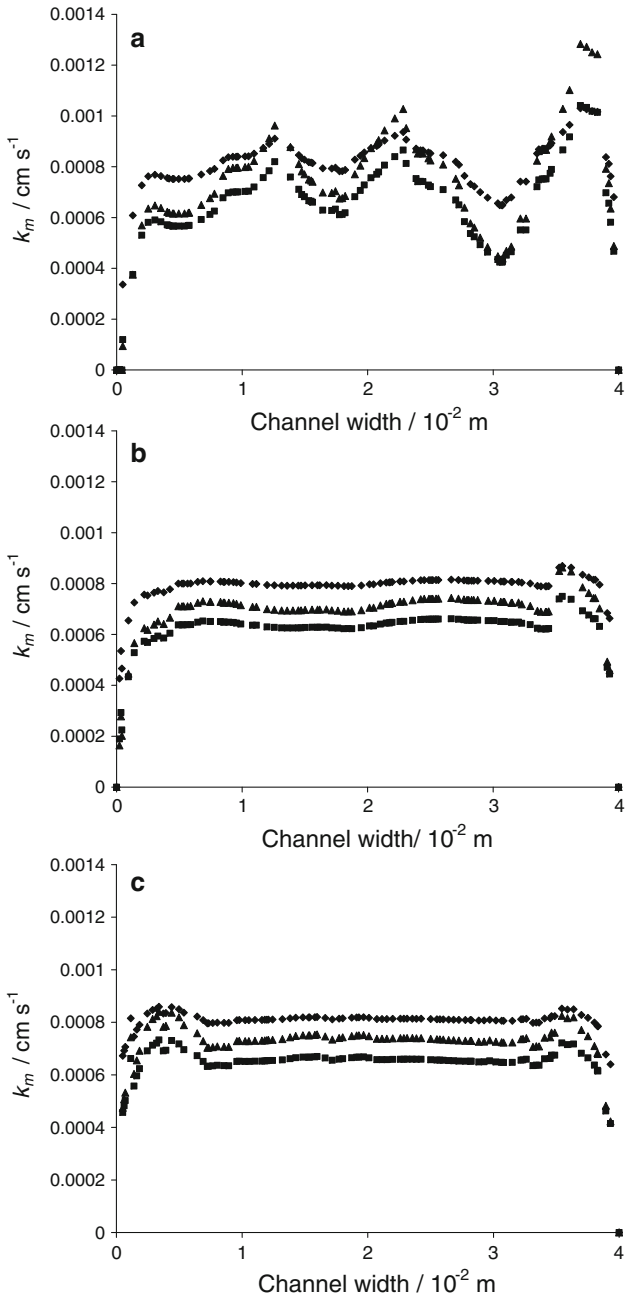

Fig. 5 Computed local k_m values for a mean linear flow velocity of 0.024 m s^{-1}, at various positions along the width of the flow channel at **a** 0.01 m, **b** 0.04 m and **c** 0.08 m from the channel entrance. Equations (18) *filled diamond*, (21) *filled square* and (22) *filled triangle*. Values are taken from Table 3

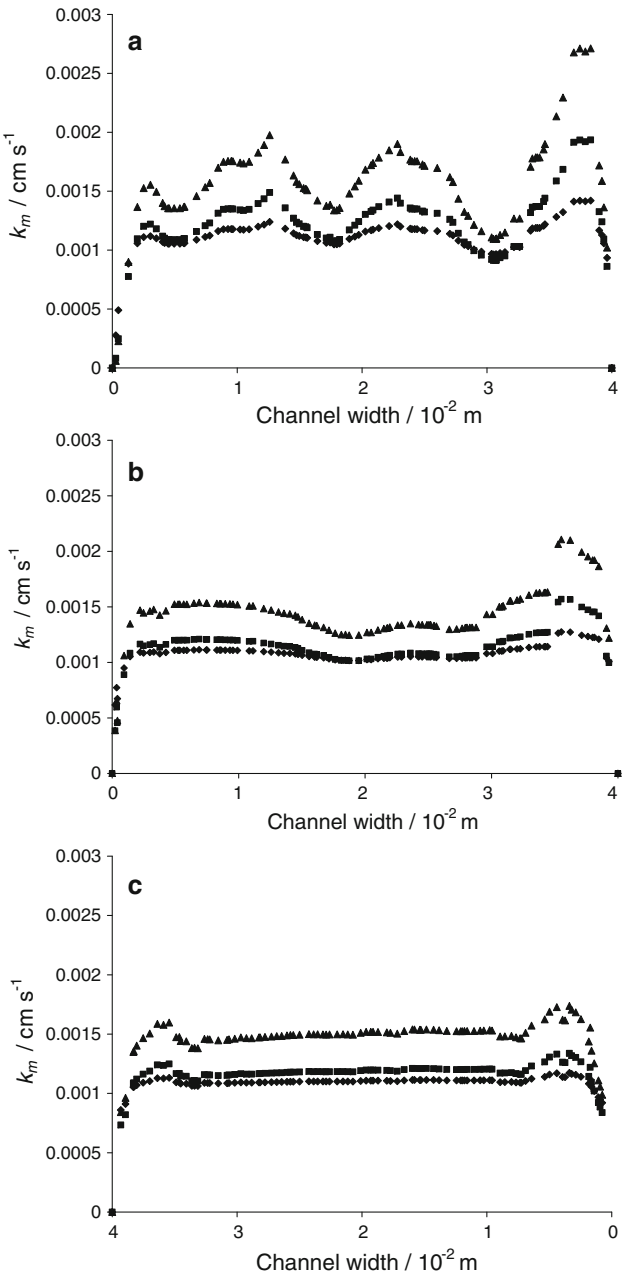

Fig. 6 Computed local k_m values for a mean linear flow velocity of 0.065 m s^{-1}, at various positions along the width of the flow channel at **a** 0.01 m, **b** 0.04 m and **c** 0.08 m from the channel entrance. Equations (18) *filled diamond*, (21) *filled square* and (22) *filled triangle*. Values are taken from Table 3

values with respect to Eq. (22): 21 and 27 %, respectively. For an imaginary electrode (0.003 m length and 0.04 m width), the following values are obtained: Eq. (21), averaged $k_m = 1.16 \times 10^{-3}$ cm s^{-1} (RE of 24.7 % against the experimental 1.54×10^{-3} cm s^{-1}) and Eq. (18), averaged $k_m = 1.08 \times 10^{-3}$ cm s^{-1} (RE of 28.9 % against the experimental). The conclusion so far is that at a nominal *Re* of 533, the effect of the manifold configuration on the mass transport coefficient is estimated with the same precision by both Eqs. (18) and (22). However, Eq. (22) gives k_m values 5 % higher than Eq. (18).

5.4 Mean linear flow velocity, $v = 0.097$ m s^{-1}

Under these hydrodynamic conditions, turbulent structures are further increased. Accordingly, for the first third of the

channel length, a non-uniform k_m distribution is expected. Figure 7a shows the corresponding set of k_m at 1 cm from the channel entrance. Perceptible differences in their calculations are found at jets' positions where the maximum REs are 32 and 55.6 %, corresponding to Eqs. (21) and (18). For an imaginary electrode (0.003 m length and 0.04 m width), the following values are obtained: Eq. (21), averaged $k_m = 1.53 \times 10^{-3}$ cm s^{-1} (RE of 26.8 % against the experimental 2.09×10^{-3} cm s^{-1}) and Eq. (18), averaged $k_m = 1.23 \times 10^{-3}$ cm s^{-1} (RE of 41 % against the experimental value).

Figure 7b shows a set of local mean mass transport coefficients along the channel width at 4 cm from the channel entrance. Equation (18) predicts a smoother k_m distribution than Eq. (21). If it is considered that the set of k_m evaluated by Eq. (22) is the most realistic, for these conditions, errors of Eq. (18) are in the range of 28.6 % < RE < 51.2 %, whilst errors of Eq. (21) are in the range 1 % < RE < 30.2 %. For an imaginary electrode (0.003 m length and 0.04 m width), the following values are obtained: Eq. (21), averaged $k_m = 1.46 \times 10^{-3}$ cm s^{-1} (RE of 28.7 % against the experimental 2.09×10^{-3} cm s^{-1}) and Eq. (18), averaged $k_m = 1.22 \times 10^{-3}$ cm s^{-1} (RE of 41.6 % against the experimental value).

Figure 7c shows the corresponding set of k_m at 8 cm from the channel entrance. The set of k_m is uniform, except near the channel boundaries where the wall effects are noticeable for Eqs. (21) and (22), but not for Eq. (18). If it is considered that the set of k_m evaluated by Eq. (22) is the most realistic, for this condition, errors of Eq. (18) are in the range of 37.9 % < RE < 42.7 %, whilst errors of Eq. (21) are in the range of 24.6 % < RE < 24.8 %. For an imaginary electrode (0.003 m length and 0.04 m width), the following values are obtained: Eq. (21), averaged $k_m = 1.49 \times 10^{-3}$ cm s^{-1} (RE of 28.7 % against the experimental 2.09×10^{-3} cm s^{-1}) and Eq. (18), averaged $k_m = 1.24 \times 10^{-3}$ cm s^{-1} (RE of 40.7 % against the experimental). At this stage, the findings could be summarised that at high nominal *Re* numbers, the effect of the manifold configuration on the mass transport coefficient is best estimated by Eq. (21).

5.5 The flow pattern and mass transport correlation

It can be seen from the previous section that numerical simulation of a realistic flow pattern provides a very useful tool for predicting mass transport coefficients in a reactor channel, provided an appropriate mass transport correlation is selected. From the lowest characteristic linear flow velocity (0.024 m s^{-1}) to the highest one (0.097 m s^{-1}) considered in this work, the RE of the Eq. (18) has constantly increased, whilst the RE of Eq. (21) was almost constant. This implies that Eq. (21) is better than Eq. (18) over the entire *Re* range studied.

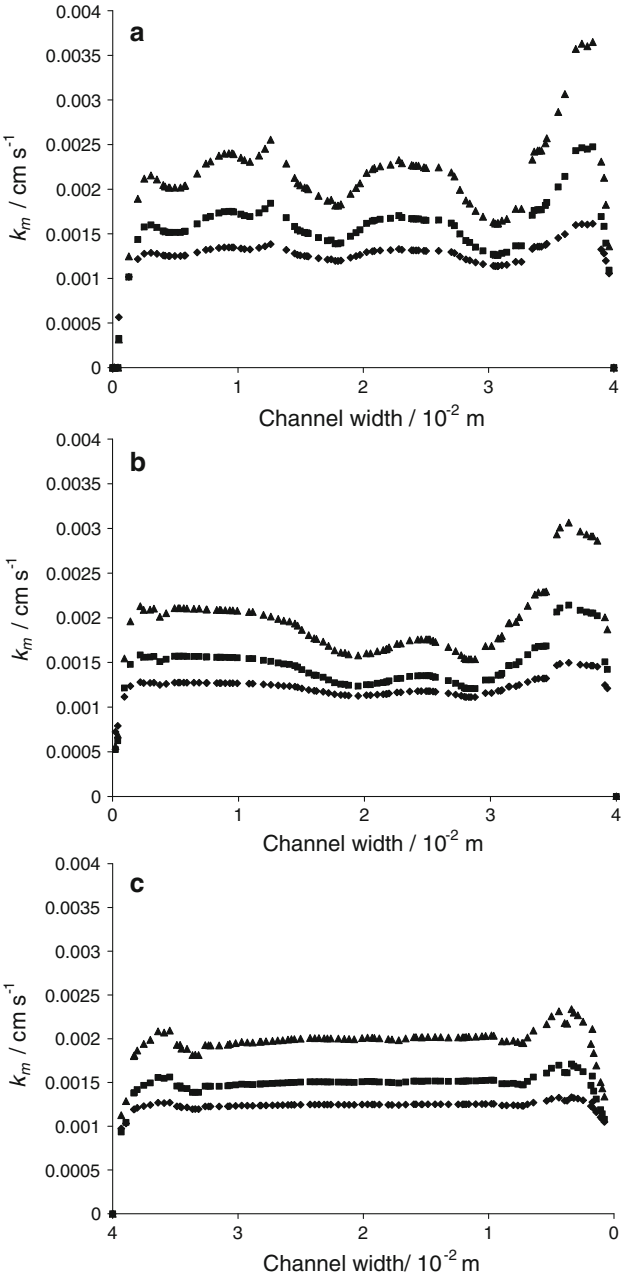

Fig. 7 Computed local k_m values for a mean linear flow velocity of 0.096 m s^{-1}, at various positions along the width of the flow channel at **a** 0.01 m, **b** 0.04 m and **c** 0.08 m from the channel entrance. Equations (18) *filled diamond*, (21) *filled square* and (22) *filled triangle*. Values are taken from Table 3

Applying the procedure described above, mass transport coefficients were theoretically evaluated, in the whole channel, for a wide range of experimental characteristic linear flow velocities (in the range of 0.024 and 0.11 m s^{-1}) using the mass transport correlations shown in Table 3. Figure 8 shows 5 numerical sets and 1 experimental set of k_m values versus the characteristic mean linear electrolyte velocity. The most appropriate mass

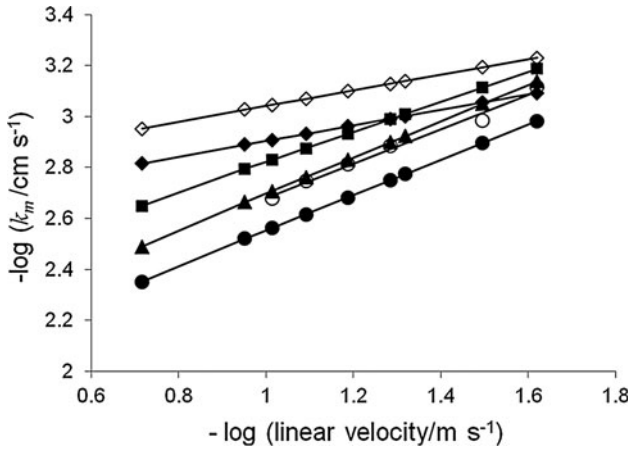

Fig. 8 Log-log plot of computed mass transport coefficient versus mean linear flow velocity. Five numerical data sets (curves *filled diamond*, *open diamond*, *filled circle*, *filled square*, *filled triangle*,) and one experimental data set (*open circle*) are compared in the mean linear velocity range 0.024–0.192 m s^{-1}. Table 3 provides further details of the conditions. *filled diamond* ideal fully developed laminar flow [3, 18] from Eq. (18); *open diamond* fully developed laminar flow, at infinitely wide electrodes [3] from Eq. (19), *filled circle* mass transport correlation for a baffled reactor [46] from Eq. (20), *filled square* mass transport correlation for a flat plate [3] from Eq. (21); *filled triangle* empirical correlation experimentally found for the FM01-LC reactor [10] from Eq. (22)

transport correlation is the empirical one experimentally found for the FM01-LC reactor according to Eq. (22). When this correlation is coupled with a theoretical flow pattern, the mass transport coefficient (k_m) can be predicted within an experimental error RE $\leq$ 6 %. The following best equation is the flat plate mass transport correlation (Eq. 21). By means of this equation, mass transport coefficient (k_m) can be predicted within 18 % $<$ RE $<$ 28.7 %.

The other mass transport correlations give poor mass transport coefficient predictions with the following errors ranges: baffled parallel plate reactor according to Eq. (20), -22.8 % $<$ RE $<$ -36.6 %; ideal fully developed laminar flow in Eq. (18), -5.4 % $<$ RE $<$ 40.9 %; and finally the worst errors were found for the fully developed laminar flow, assuming infinitely wide electrodes in Eq. (19), namely 23.3 % $<$ RE $<$ 56.9 %.

6 Conclusions

A novel numerical procedure for a realistic mass transport coefficient (k_m) prediction has been successfully applied to a parallel plate electrochemical laboratory reactor.

The effect of the manifold configuration on the mass transport coefficient can be evaluated by coupling a realistic flow pattern with a mass transport correlation. In this fashion, mass transport coefficients were numerically evaluated with acceptable accuracy (18 % $<$ RE $<$ 28.7 %) over the entire FM01-LC reactor, using a wide range of experimental flow velocities from 0.024 to 0.11 m s^{-1}.

A major feature of this approach is the minimal time and number of physical parameters needed for a rapid reliability test to simulate the mass transport coefficient in the FM01-LC reactor. This approach could be useful in reactor design since it facilitates a rapid preliminary characterisation of electrochemical reactors.

In order to further scrutinise the accuracy of the RNG turbulence model applied to this numerical procedure, further work should couple more turbulence models to the set of Navier–Stokes equations followed by a critical evaluation of the computational results against experimentally measured values.

Acknowledgements This paper is dedicated to the memory of our colleague Dr. José Gonzalez-Garcia (1963–2012) of the University of Alicante; we have valued his colleagueship and electrochemical engineering contributions to mass transport and fluid flow characterisation of filter-press reactions over many years.

References

1. Goodridge F, Scott K (1995) Electrochemical process engineering. A guide to the design of electrolytic plant. Plenum Press, New York
2. Hammond JK, Robinson D, Brown CJ, Pletcher D, Walsh FC (1991) Mass transport studies in filterpress monopolar (FM-type) electrolysers. II-Laboratory studies in the FM01-LC reactor. In: Kreysa G (ed) Electrochemical cell design and optimization procedures. Dechema monographs, vol 123. Wiley-VCH, Weinheim, pp 299–315
3. Walsh FC (1993) A first course in electrochemical engineering. The Electrochemical Consultancy, Romsey
4. Pletcher D, Walsh FC (1993) Industrial electrochemistry. Blackies, London
5. Wendt H, Kreysa G (1999) Electrochemical engineering, science and technology in chemical and other industries. Springer Verlag, Berlin
6. Ponce de León C, Reade GW, Whyte I, Male SE, Walsh FC (2007) Characterization of the reaction environment in a filter-press redox flow reactor. Electrochim Acta 52:5815–5823
7. Frías-Ferrer A, González-García L, Sáez V, Ponce de León C, Walsh FC (2008) The effects of manifold flow on mass transport in electrochemical filter-press reactors. AIChE J 54:811–823
8. Pickett DJ (1979) Electrochemical reactor design. Elsevier, Amsterdam
9. Hammond JK, Robinson D, Walsh FC (1991) Mass transport studies in filterpress monopolar (FM-type) electrolysers. I-Pilot scale studies in the FM21-SP reactor. In: Kreysa G (ed) Electrochemical cell design and optimization procedures. Dechema monographs, vol 123. Wiley-VCH, Weinheim, pp 279–297
10. Brown CJ, Pletcher D, Walsh FC, Hammond JK, Robinson D (1992) Local mass transport effects in the FM01 laboratory electrolyser. J Appl Electrochem 22:613–618
11. Brown CJ, Pletcher D, Walsh FC, Hammond JK, Robinson D (1993) Studies of space-averaged mass transport in the FM01-LC laboratory electrolyser. J Appl Electrochem 23:38–43

12. Brown CJ, Pletcher D, Walsh FC, Hammond JK, Robinson D (1994) Studies of three-dimensional electrodes in the FM01-LC laboratory electrolyser. J Appl Electrochem 24:95–106
13. Brown CJ, Walsh FC, Pletcher D (1995) Mass transfer and pressure drop in a laboratory filterpress electrolyser. Chem Eng Res Des 73a:196–205
14. Trinidad P, Walsh FC (1996) Hydrodynamic behaviour of the FM0-LC reactor. Electrochim Acta 4:493–502
15. Griffiths M, Ponce de León C, Walsh FC (2005) Mass transport in the rectangular channel of a filter-press electrolyzer (the FM0-LC Reactor). AIChE J 51:682–687
16. Trinidad P, Ponce de León C, Walsh FC (2006) The application of flow dispersion models to the FM01-LC laboratory filter-press reactor. Electrochim Acta 52:604–613
17. Vázquez L, Alvarez-Gallegos A, Sierra FZ, Ponce de León C, Walsh FC (2010) Simulation of velocity profiles in a laboratory electrolyser using computational fluid dynamics. Electrochim Acta 55:3437–3445
18. Vázquez L, Alvarez-Gallegos A, Sierra FZ, Ponce de León C, Walsh FC (2010) Prediction of mass transport profiles in a laboratory filter-press electrolyser by computational fluid dynamics modelling. Electrochim Acta 55:3446–3453
19. Walsh FC, Robinson D (1998) Electrochemical filter-press reactors. Interface 7:40–45 published by The Electrochemical Society, Inc
20. Pickett DJ, Wilson CJ (1982) Mass transfer in a parallel plate electrochemical cell-the effect of change of flow cross-section at the cell inlet. Electrochim Acta 27:591–594
21. Janna WS (1998) Internal incompressible viscous flow. In: Johnson RW (ed) The handbook of fluid dynamics. Springer-Verlag, Heidelberg
22. Levenspiel O (1972) Chemical reaction engineering. Wiley, New York
23. Shah YT, Stiegel GJ, Sharma U (1978) Backmixing in gas-liquid reactors. AIChE J 24:369–400
24. Riemer M, Kristensen G, Harremoes HP (1980) Residence time distribution in submerged biofilters. Water Res 14:949–958
25. Jimenez B, Noyola A, Capdeville B, Roustan M, Faup G (1988) Dextran blue colorant as a reliable tracer in submerged filters. Water Res 22:1253–1257
26. Jimenez B, Noyola A, Capdeville B (1988) Selected dyes for residence time distribution evaluation in bioreactors. Biotechnol Tech 2:77–82
27. Krall KM, Sparrow EM (1966) Turbulent heat transfer in the separated, reattached, and redevelopment regions of a circular tube. J Heat Transf 88:131–138
28. Filetti EG, Kays WM (1967) Discussion: heat transfer in separated, reattached, and redevelopment regions behind a double step at entrance to a flat duct. J Heat Transf 89:163–167
29. Zemanick PP, Dougall RS (1970) Local heat transfer downstream of abrupt circular channel expansion. J Heat Transf 92:53–59
30. Baughn JW, Hoffman NA, Takahashi NA, Launder BE (1984) Local heat transfer downstream of an abrupt expansion in a circular channel with constant wall heat flux. J Heat Transf 106: 789–796
31. Runchal AK (1971) Mass transfer investigation in turbulent flow downstreams of sudden enlargement of a circular pipe for very high Schmidt numbers. Int J Heat Mass Transf 14:781–792
32. Tagg DJ, Patrick MA, Wragg AA (1979) Heat and mass transfer downstream of abrupt nozzle expansions in turbulent flow. Trans Inst Chem Eng 57:176–181
33. Wragg AA, Tagg DJ, Patrick MA (1980) Diffusion-controlled current distributions near cell entries and corners. J Appl Electrochem 10:43–47
34. Rizk TY, Thompson GE, Dawson JL (1996) Mass transfer enhancement associated with sudden flow expansion. Corros Sci 38:1801–1814
35. Djati A, Brahimi M, Legrand J, Saidani B (2001) Entrance effect on mass transfer in a parallel plate electrochemical reactor. J Appl Electrochem 31:833–837
36. Pellerin E, Michelistsch E, Darcovich K, Lin S, Tam CM (1995) Turbulent transport in membrane modules by CFD simulation in two dimensions. J Memb Sci 100:139–153
37. Karniadakis GE, Mikic BB, Patera AT (1988) Minimum-dissipation transport enhancement by flow destabilization: Reynolds' analogy revisited. J Fluid Mech 192:365–391
38. Cao Z, Wiley DE, Fane AG (2001) CFD Simulation of net-type turbulence promoters in a narrow channel. J Memb Sci 185: 157–176
39. Ahmad LA, Lau KK, Abu Bakar MZ, Abd Shukor SR (2005) Integrated CFD simulation of concentration polarization in narrow membrane channel. Comput Chem Eng 29:2087–2095
40. Vivek V, Ranade W, Kumar AJ (2006) Fluid dynamics of spacer filled rectangular and curvilinear channels. Memb Sci 271:1–15
41. Versteeg HK, Malalasekera W (2007) An introduction to computational fluid dynamics. Pearson Prentice Hall, Essex
42. Fluent in User's Guide (2003) Fluent Inc., Lebanon
43. Angioletti M, Di Tommaso RM, Nino E, Ruocco G (2003) Simultaneous visualization of flow field and evaluation of local heat transfer by tranitional impinging jets. Int J Heat Mass Trans 46:1703–1713
44. Klemm T, Gabi M (2003) Using PIV and CFD to investigate the effect of casing design on cross flow fan performance. In: Proceedings of PSFVIP-4 (F4013), Chamonix, France, 3–5 June 2003
45. Bard AJ, Faulkner LR (1980) Electrochemical methods. Fundamentals and applications. Willey, New York
46. Goodridge F, Mamoor GM, Plimley RE (1986) Mass transfer rates in baffled electrolytic cells. I Chem E Symp Ser 98:61–68
47. Rabinovich S (1995) Measurement errors, theory and practice. AIP Press, New York